Crystallizing elusive chromium polycations

Wei Wang[1], Lauren B. Fullmer[1], Nuno A. G. Bandeira[2,3], Sara Goberna-Ferrón[1], Lev N. Zakharov[1], Carles Bo[2,3]*, May Nyman[1,*] and Douglas A. Keszler[1,*]

[1]Center for Sustainable Materials Chemistry, Department of Chemistry, 153 Gilbert Hall, Oregon State University, Corvallis, Oregon 97331-4003, USA

[2]Institute of Chemical Research of Catalonia, ICIQ, Tarragona, Av. dels Països Catalans, 16, 43007, Spain

[3]Departament de Química Física i Inorgànica, Universitat Rovira i Virgili, Av. dels Països Catalans, 26, 43007 Tarragona, Spain

*Correspondence to: douglas.keszler@oregonstate.edu; may.nyman@oregonstate.edu; cbo@iciq.cat

SUMMARY

Oxo and oxo-hydroxo metal clusters are commonly isolated from aqueous solutions with capping ligands to prevent precipitation of metal hydroxides. Few simple molecular oxo-hydroxo metal clusters are readily synthesized and isolated without these capping ligands. Yet uncapped clusters are important in metal oxide growth and for applications hindered by auxiliary ligands. Uncapped clusters containing transition metals with partially filled *d* shells are especially difficult to prepare – they rapidly aggregate and precipitate, preventing isolation of the initial cluster form. Herein, we elucidate a cluster self-assembly and crystallization process that has yielded a new uncapped oxo-hydroxo cluster containing Zn^{2+}, Al^{3+}, and the open-shell transition metal ion Cr^{3+}, i.e., $[ZnO_4Al_{5.1}Cr_{6.9}(OH)_{24}(H_2O)_{12}Zn(H_2O)_3]^{8+}$. For decades, clusters of Cr^{3+} and Zn^{2+} have been synthesis targets in polyoxocation chemistry, but they have resisted isolation and crystallization. We control pH-driven hydrolysis by oxidative dissolution of zinc in the reaction solution, rather than by addition of hydroxide. The control gained by Zn dissolution allows metal nitrate concentrations 10× higher than conventional hydroxide addition. Therefore, a high nitrate concentration further suppresses cluster self-assembly in the bulk. Contrary to common cluster growth studies, the fully assembled cluster is not observed spectroscopically in the bulk reaction solution from which the clusters are crystallized. Instead, the reaction solution is dominated by monomeric and dimeric metal species, even while the solution actively grows crystals. Evaporation of the HNO_3-H_2O azeotrope at the solution surface allows simultaneous cluster self-assembly and crystallization. Because these reactive clusters do not accumulate in the bulk solution and are isolated by crystallization, the state that often results in uncontrolled precipitation of metal hydroxide is avoided. The proposed formation pathway opens new opportunities to explore and augment the composition space and reaction chemistry of

compositionally complex oxo-hydroxo clusters, particularly those comprising metals with partially filled *d* shells.

The Bigger Picture

Aqueous metal-oxide clusters are important in natural processes, in synthesis, and in technology. In nature, they are central to contaminant transport, mineral growth, photosynthesis, and biomineralization. In synthesis, they provide nanometric forms with size dependent properties, and they are pre-assembled building blocks for materials. Fabricating functional metal oxide clusters and cluster-based materials in water minimizes environmental impact. Clusters synthesized and manipulated in water provide understanding of natural processes and inspire biomimetic materials; i.e. for artificial photosynthesis.

While synthesis of functional clusters is accomplished with great control in organic solvents; it doesn't offer the simplicity and sustainability of aqueous synthesis. But aqueous syntheses that provide well-controlled cluster and material growth are not well-developed. The unique cluster formation processes created in this study opens the door to new understanding of natural processes and unprecedented control of aqueous synthesis.

INTRODUCTION

Simple molecular oxo-hydroxo metal clusters, assembled in water *without* stabilizing organic ligands, are building blocks for both natural and synthetic metal oxides (Baumgartner et al., 2013; Gebauer et al., 2008; Habraken et al., 2013; Sadeghi et al., 2015). Molecular clusters function as homogeneous catalysts;(Barats et al., 2008; Kamata et al., 2003; Yin et al., 2010) separation reagents for environmental,(Stewart et al., 2009) energy,(Wylie et al., 2014) and biomedical applications;(Lee et al., 2005) and in crystallization of biomolecules(Bashan and Yonath, 2008). Controlling cluster reactivity has led to breakthroughs in their use as precursors for thin-film deposition (Anderson et al., 2007) and high-resolution nanopatterning (Oleksak et al., 2014). Amongst all metals in the periodic table, only oxo-hydroxo clusters of Al^{3+}, Ga^{3+}, U^{6+}, and the d^0 transition metals V^{5+}, Nb^{5+}, Ta^{5+}, Mo^{6+}, and W^{6+} are readily isolated in stable forms without supporting organic or inorganic ligands.(Casey, 2006; Nyman and Burns, 2012; Pope, 1983) Certainly ligation plays an important role in inorganic and materials chemistry, as well as geochemistry. For example, organic ligands provide a mechanism to stabilize clusters that form in water, yielding structural information that is important to elucidate aqueous reactivity and speciation of metal cations.(Lokare et al., 2016; Sadeghi et al., 2015) Organic ligands are historically and currently valuable to isolate transition metal and lanthanide single-molecule magnet clusters that possess unique magnetic behavior. (Ako et al., 2006; Baskar et al., 2007; Newton et al., 2011) Inorganic ligands (POM fragments, oxoanions) are also used to capture transient polynuclear forms to elucidate speciation (Izarova et al., 2014; Izarova et al., 2010; Son et al., 2015) and provide water-soluble cluster forms, for catalysis for instance.(Stracke and Finke, 2011; Yin et al., 2010) Inorganic oxoanion ligands link clusters into functional open-framework materials.(Sun et al., 2011) However, many applications are hindered by ligands. To advance the use of discrete clusters in medicine,(Rhule et al., 1998) technology,(Busche et al., 2014; Llordes et al., 2013) and other important applications, we must determine how to isolate clusters of any metal in the periodic table without the use of chemistry-limiting ligands.

pH-dependent speciation diagrams from decades of research(Baes and Mesmer, 1976) convincingly show 1) cluster assembly in water is controlled predominantly by

pH and concentration, 2) clusters generally revert to monomers or aggregates and precipitates outside a specific pH stability window, and 3) clusters must be abundant in solution before crystallization (as an important purification step) can proceed. Hence, clusters existing only in narrow pH and concentration windows are very difficult to isolate. Clusters of open-shell transition metals fall into this class, because the partially filled *d* shell promotes the reactivity of coordinated aqua ligands(Winkler and Gray, 2012), causing uncontrolled hydrolysis and condensation.

Here, we demonstrate isolation via crystal growth of a discrete mixed-metal cluster containing the open-shell transition-metal Cr^{3+}. We show that the cationic cluster $[ZnO_4Al_{5.1}Cr_{6.9}(OH)_{24}(H_2O)_{12}Zn(H_2O)_3]^{8+}$, onward abbreviated $Zn(CrAl)_{12}$, is readily isolated in single-crystal form as a nitrate salt, but we never observe pre-assembly in solution. Cluster formation *in solution* is suppressed by excess nitrate, which stabilizes monomeric or dimeric aqua metal cations instead. Removal of nitrate by evaporation of the HNO_3-H_2O azeotrope drives cluster formation only as a crystalline solid. This 'classical' growth mechanism, a description of metal oxide formation without polynuclear cluster assembly prior to crystallization, bypasses the unstable solution cluster state that usually results in aggregation and production of an insoluble hydroxide(Baumgartner et al., 2013; Gebauer et al., 2014; Gebauer et al., 2008; Habraken et al., 2013). Crystallization of clusters without initial persistence in solution has not previously been considered as a way to isolate highly reactive clusters. The synthetic strategy employed here exploits both a slow hydrolysis process (by oxidative dissolution of zinc in the metal nitrate solution), and heterogeneous solution conditions that presumably only allows condensation reactions at the liquid-air interface, where rapid crystallization is also seeded. However once the $Zn(CrAl)_{12}$ cluster is isolated in the solid-state lattice, it is stable, and can be redissolved, characterized and exploited in different solvents including water and dimethylformamide.

On the other hand, isolation of the $Zn(CrAl)_{12}$ cluster simply provides two important advances in polyoxocation chemistry. First, the Cr polycation Keggin ion (or related cluster) was long thought to exist as an aqueous specie, but prior attempts of its isolation proved unsuccessful. (Bradley et al., 1993) Second, Zn in the center of the Keggin ion was predicted to offer stabilization of polycationic Keggin ions;(Parker et al., 1997; Stewart et al., 2009) but again, this could not be proven without definite structural evidence. Isolation and structural characterization of $Zn(CrAl)_{12}$ has now provided opportunity to probe via computation and experiment the stability of chromium polycations, as well as the effect of the Zn-center, the Zn-cap and more broadly, the relationship between capping Keggin ions and rotational isomerization.

EXPERIMENTAL PROCDURES

Synthesis of $Zn(CrAl)_{12}$. The reaction solution was prepared by dissolving $Al(NO_3)_3{\cdot}9H_2O$ (1.69 g) (BAKER ANALYZED Reagent, ACS Grade) and $Cr(NO_3)_3{\cdot}9H_2O$ (0.60 g) (Alfa Aesar, 99.99% (metals basis)) in Millipore H_2O (= 18.2 MΩ*cm) to make a 10-mL solution (0.45 M Al^{3+}(aq.) and 0.15 M Cr^{3+}(aq.)). Zinc metal powder (0.20 g, 0.3M concentration) (Alfa Aesar, -140+325 mesh, 99.9% metals basis) was then added to this clear solution. The molar ratio between Zn and (Al+Cr) was 1:2, and total metal concentration is 0.9 M. The reaction mixture was stirred overnight and the clear solution was then filtered into a small vial and placed in ambient condition for evaporation. Numerous dark-green crystals were formed after two to three weeks. Yield ~70% based on Cr.

Monitoring Reaction Solutions with Heating. To investigate the reaction pathway, we also carried out the synthesis with heating (40, 50, 60, 70 and 80 °C).

Both X-ray scattering and electrospray mass spectrometry (see below) was used to monitor these reaction solutions. We also collected the vapors that distilled from these heated solutions via condensation, and this solution was characterized by Raman spectroscopy (Thermo Scientific DXR SmartRaman spectrometer, 780 nm laser source). Solutions contained in a glass vial was placed on the sample window for data collection; step size: 1 cm^{-1}, range: 600-1000 cm^{-1}, number of scans: 8, exposure time: 2 seconds.

Single crystal X-ray diffraction data for $Zn(CrAl)_{12}$: $H_{54}N_8O_{67}Zn_2Al_{5.10}Cr_{6.90}$, $(OH)_{24}(H_2O)_{15}(NO_3)_8O_4$ $Zn_2Al_{5.10}Cr_{6.90}$, MW = 1865.62 (not including lattice water), 0.18 x 0.18 x 0.04 mm, T = 173(2) K, Rhombohedral, space group R-3*m*, a = b = 18.502(2) Å, c = 32.090(6) Å, □ = β = 90°, □ = 120°, V = 9513(2) $Å^3$, Z = 6, D_c = 1.973 Mg/m^3, μ = 2.087 mm^{-1}, F(000) = 5687, 2□$_{max}$ = 54°, 2539 independent reflections [R_{int} = 0.0158], R_1 = 0.0479, wR_2 = 0.1603 and GOF = 1.035 for 2539 reflections (107 parameters) with I>2s(I), R_1 = 0.0548, wR_2 = 0.1710 and GOF = 1.035 for all reflections, max/min residual electron density +0.693/-0.687 $Å^3$ **Further details**. All non-H atoms were refined with anisotropic thermal parameters; and H atoms were not directly located. It was found that Al and Cr atoms share three symmetrically independent positions: CrAl1, CrAl2 and CrAl3. The final refinement of the structure was done based on the Cr:Al ratios (0.89:0.11 for CrAl1; 0.68:0.32 for CrAl2 and 0.37:0.63 for CrAl3) obtained from bond valance calculation. Eight NO_3 anions and solvent water molecule in the structure are disordered and were treated by SQUEEZE(Van der Sluis and Spek, 1990). Correction of the X-ray data by SQUEEZE yielded 258 electrons, that is close to the required value of 256 electrons for eight NO_3^- anions in the symmetrically independent part. The structure is deposited in the ICSD (Karlsruhe, DE; CSD-428054)

Electron Microprobe Analysis (EPMA). Data was collected using a Cameca SX-50 with wavelength dispersive spectrometers and gas-flow proportional detectors with P-10 gas; electrons were accelerated under 10, 15, and 20 kV and the generated K□ line intensity of Zn, Al, Cr, N, and O were recorded during the measurement. Measurement was done at six different positions on the crystal. Zn metal, Al metal, Cr metal, AlN, and MgO were used as standards and a background correction was applied as described in detail by Donovan and Tingle.(Donovan and Tingle, 1996) Data analysis for was done in ProbeWin software. Note: with the proper references, this data yielded a composition consistent with bond valence sum from crystallography and free refinement of mixed occupancy Cr/Al sites (based on thermal parameters). Therefore this method is considered acceptable for compositional analysis.

Determination of water content and moiety formula. Thermogravimetric Analysis. The solvent content in $Zn(CrAl)_{12}$ crystals was determined by TGA using a Q50 TGA (TA instruments) thermogravimetric analyzer. Samples were run at a heating rate of 10°C/min up to 850°C in a nitrogen environment with a flow rate of 100 mL/min. The total weight loss is 55%, consistent with 16 water molecules. The structure has a free void space (from the checkcif) of 4951 $Å^3$. The eight nitrates per cluster plus 16 water molecules per cluster has a theoretical volume of 4896 $Å^3$, assuming 17 $Å^3$ per non-hydrogen atom. Therefore the TGA and structural analysis agree with an estimate of 16 water molecules per cluster, and a moiety formula of $[ZnO_4Al_{5.10}Cr_{6.90}(OH)_{24}(H_2O)_{12}Zn(H_2O)_3][(NO_3)_8]•16H_2O$ (MW=2153.62 including lattice water).

Electrospray ionization mass spectrometry. ESI-MS was carried out using an Agilent 6230 TOF mass spectrometer. Reaction solutions were diluted tenfold and 10 μL aliquots were injected with water as the mobile phase and flow rate of 0.4 mL/min. Fragmentation voltage, cone voltage, and octopole voltage were set at 100, 50, and 750 V respectively.

SAXS. X-ray scattering data were collected on an Anton Paar SAXSess instrument utilizing Cu-K radiation (1.54 Å) and line collimation, equipped with a 2-d image plate for data collection in the q=0.018-2.5 $Å^{-1}$ range. The sample to image-plate distance is 26.1 cm. All solutions were contained in a sealed disposable 1.5 mm diameter capillary tube, and data collection time was 30min. All solutions are filtered prior to analysis to remove large particles, dust for example. Likewise, background solutions were measured for 30 minutes. SAXSQUANT software was used for data collection and treatment (normalization, primary beam removal, background subtraction, desmearing, and smoothing to remove extra noise created by the desmearing routine). Differences in scattering intensity in the high q-range (~q>1 $Å^{-1}$) from similar solutions is the result of imperfect background subtraction, a universal problem with these small clusters. However, we found with varying processing parameters (i.e. normalization of scattering curves prior to background subtraction) gave very similar results. Therefore the data interpretation is robust. All analyses were carried out utilizing the IRENA(Ilavsky and Jemian, 2009) macros within IgorPro 6.3 (Wavemetrics) software. Simulation of scattering data was performed using SolX.(Tiede et al., 2004; Zhang et al., 2000) Initially, a .xyz file of the cluster-only is prepared (with no symmetry elements) and converted to a .pdh format for import into SolX.

Computational Details. The Amsterdam Density Functional (ADF) program package (**http://www.scm.com**, ***Scientific Computing and Modelling* ADF-2013.01**) version 2013.01 has been used throughout to opti-mize the geometries of all the species considered herein. The Becke(Becke, 1988a) and Perdew(Perdew, 1986a, b) gradient corrected exchange and correlation functionals (BP86) respectively were used in the calculations. The ZORA(van Lenthe et al., 1993; van Lenthe et al., 1999) scalar relativistic Hamiltonian was employed with a triple zeta Slater type orbit(Van Lenthe and Baerends, 2003) (STO) augmented with one polarization function (TZP) for all the atoms. A small frozen core was used for all the elements (1s2 shell for O and C, and 2p6 shell for Al, Zn) except hydrogen. The geometry optimizations were performed via the default numerical integration scheme of Becke (Becke, 1988b). Stationary points were located with the default integration accuracy and employing the COSMO implicit solvation scheme. No symmetry constraints were used. Since magnetic couplings are small and in the order of cm^{-1}, all Cr(III) derivatives were calculated as high spin open shell systems.

RESULTS

Structure

The relationship between structure (SI figures 1-3 & crystallographic information file) and composition of $Zn(CrAl)_{12}$ provides insight into its formation, as will be discussed later. It is a Zn-centered, Zn-capped -Keggin ion (Fig. 1), represented as a stacking of mixed-occupancy Cr/Al-centered octahedra: basal (blue), equatorial (magenta), and apical (teal). The occupancies of Cr and Al in these sites were determined from the X-ray structure and derived bond valence sums (BVS, Supplementary Tables 1-16). Free refinement gives Cr:Al ratios of 0.37:0.63 for the CrAl3 basal plane, 0.67:0.33 for the CrAl2 equatorial plane, and 0.89:0.11 for the CrAl1 apical plane. Hence, the average Cr:Al ratio is 6.9:5.1, consistent with electron microprobe analysis on the bulk material (Cr:Al = 6.8:5.2, Supplementary

Table 17). Metal-oxygen bond distances increase from CrAl3 (1.90 - 1.94 (3) Å) to CrAl2 (1.95 - 1.98 (3) Å) to CrAl1 (1.94 - 2.00 (3) Å) - all correlated to the larger six-coordinate ionic radius of Cr^{3+} (r = 0.76 Å) vs Al^{3+} (r = 0.68 Å). From BVS analysis, H_2O occupies the terminal positions of the Cr/Al octahedra and the Zn cap (oxygen BVS = 0.4-0.5); OH^- bridges in μ_2 and μ_3 modes (oxygen BVS ~ 1.0); and O^{2-} bridges the central Zn and neighboring Cr/Al sites (oxygen BVS ~ 2.0).

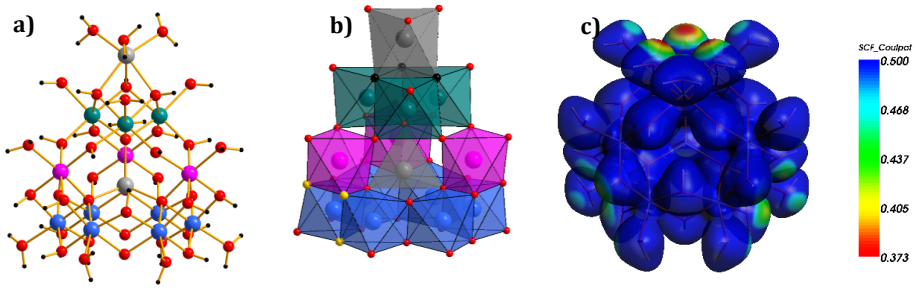

Figure 1. Views of ⍰-Zn(CrAl)$_{12}$
(A) Ball-and-stick representation with aqua and hydroxo ligands geometry-optimized from simulation (blue, pink and teal spheres are Al/Cr sites; red spheres are oxygen, black spheres are hydrogen). (B) Polyhedral representation emphasizing three crystallographically and compositionally distinct sites - CrAl3 (blue, basal), CrAl2 (magenta, equatorial), and CrAl1 (teal, apical). (C) Molecular Electrostatic Potential (MEP) mapped onto the electron density (0.02 a.u. isosurface) of hypothetical ⍰-$ZnAl_{12}$. Red colors have the least positive values (more nucleophilic) and blue the most positive. The black spheres in the polyhedral representation correspond to the more nucleophilic hydroxo ligands of the apical trimer in the MEP map. The yellow spheres correspond with the less nucleophilic hydroxo ligands associated with two blue and one magenta polyhedra.

Computational studies

Computational studies were executed to elucidate the 'ordered disorder' depicted in **figure 1b** that leads to preferential occupancy in the CrAl position next to the Zn cap. These studies also yielded a broader understanding of Keggin ion rotational isomerization.

The site preferences of Cr^{3+} among the three nonequivalent octahedral positions have been elucidated by theory. The observed ~7:5, Cr:Al ratio leads to an intractable number of isomers for computation. Therefore, we modeled the cluster as a ⍰-Keggin with the metal composition $ZnAl_6Cr_6$. This formulation is similar to the experimentally determined composition, but it sets a manageable number of isomers⍰ sixteen (Table 1). The degeneracy of each isomer is derived from combinatorial algebra: taking *m* Cr atoms in CrAl3, *n* in CrAl2, and *l* in CrAl1, the total number of isoenergetic structures will be $\left(\frac{6}{m}\right) \times \left(\frac{3}{n}\right) \times \left(\frac{3}{l}\right)$, where $n + l + m = 6$. All positional isomers and corresponding degeneracy (number of Cr/Al arrangements within the three layers, Supplementary Figs. 4 & 5), relative energy, and Boltzmann weight are compiled in Table 1. Boltzmann weight is defined in the Supplementary Information, along with additional isomers that were considered for those lowest-energy structures, confirming the hypothesis that Cr/Al arrangement within layers is less important.

The energetically most stable arrangements correspond to those with the highest Cr contents in the equatorial and apical layers (0/3/3, 1/2/3, and 1/3/2). Analysis employing the Boltzmann distribution yields a Cr population of 92% for the three lowest energy isomers. The highest Boltzmann weight (55.3%) does not correspond to the lowest energy structure because of the large number of degenerate structures. Considering the Boltzmann weight of a given structure, the mean theoretical occupancies of each metal atom per layer is determined (see Supplementary Information). The agreement between simulated and experimental compositions is remarkable (Table 1, bottom). The largest deviation is in the basal

layer, where a simulated Cr occupancy of 15% compares with an experimental value of 37%. This result is an artifact of our simplified computational model, which assumes a lower Al content than observed experimentally.

Table 1. Relative energies (ΔE) of simulated CrAl site occupancies for the ⍻-$ZnCr_6Al_6$ model

Cr content basal/equatorial/apical	Degeneracy(g_i)	ΔE (kJ.mol^{-1})	Boltzmann weight
Cr-6/0/0	1	64	1.20×10^{-12}
Cr-5/1/0	18	50	6.83×10^{-9}
Cr-5/0/1	18	52	2.25×10^{-9}
Cr-4/2/0	30	35	4.01×10^{-6}
Cr-4/0/2	30	41	3.49×10^{-7}
Cr-4/1/1	135	43	7.82×10^{-7}
Cr-3/3/0	20	25	0.000167
Cr-3/0/3	20	25	0.000126
Cr-3/2/1	180	22	0.00551
Cr-3/1/2	180	29	0.000283
Cr-2/3/1	45	20	0.00251
Cr-2/1/3	45	13	0.0442
Cr-2/2/2	135	17	0.0246
Cr-1/2/3	18	4	0.553
Cr-1/3/2	18	7	0.197
Cr-0/3/3	1	0	0.172
Total	894		1

Crystallographic site	Calculated CrAl site occupancy for the ⍻-$ZnCr_6Al_6$ model		Experimental CrAl site occupancy for $Zn(CrAl)_{12}$	
	% Cr	% Al	%Cr	%Al
CrAl1	92	8	89	11
CrAl2	78	22	68	32
CrAl3	15	85	37	63

Hirshfeld charges, q,(Hirshfeld, 1977) of the hydroxo ligands in the apical plane of simulated Al_{13}, $ZnAl_{12}$, and $ZnCr_{12}$ δ isomers are slightly more negative (q_o = -0.302) than the other hydroxo ligands in the cluster (q_o = -0.285). This result is illustrated visually in the Molecular Electrostatic Potential (MEP) of δ-$ZnAl_{12}$ (Fig. 1c). The capping of the cluster by $(Zn(H_2O)_3)^{2+}$ can therefore be rationalized as a consequence of the additional nucleophilic character of the hydroxo ligands in the apical trimer. Moreover, the computed nucleophilicity of the hydroxo ligands in the apical plane is consistent with the observation that all δ-Keggin polycation isomers and derivatives are capped by an additional metal ion.(Allouche et al., 2001; Rowsell and Nazar, 2000) To further consider the selectivity of Cr over Al in the apical plane, fragment analyses of hypothetical δ-$ZnAl_{12}$ and δ-$ZnCr_{12}$ with the $(Zn(H_2O)_3)^{2+}$ cap were performed. These analyses revealed a considerable difference in interaction energies, i.e., 152 kJ·mol^{-1} in favor of δ-Zn_2Cr_{12} over δ-Zn_2Al_{12}. This result indicates a thermodynamic preference for association of the $(Zn(H_2O)_3)^{2+}$ cap with a Cr-rich apical plane. Overall, the computations show the preferred apical-plane occupation by Cr drives the experimentally-observed site ordering.

We conclude the computational discussion with consideration of the stabilization effect of ZnO_4 as a templating central polyhedron of the Keggin ion compared to AlO_4 (Table 2). For all rotational isomers, the AlO_4-centered cluster was more stable than the ZnO_4-centered cluster. While this calculation is consistent with the fact that the ZnO_4-centered Keggin ion could not be prior isolated; it is inconsistent with the

results of these synthetic experiments in which only ZnO_4 occupies the center of the Keggin ion. This is a fact confirmed by ^{27}Al NMR of dissolved $Zn(CrAl)_{12}$ crystals, which did not show the typical tetrahedral AlO_4 at 62 ppm, observed in ^{27}Al NMR spectra of aqueous tridecameric Al_{13} Keggin ion. The pH of the reaction solution (2.0-2.5) is probably too low to possess abundant AlO_4, compared to pH=4.0-4.5 solutions from which AlO_4-centered aluminum polycation Keggin ion is isolated. This is also the emerging explanation for conditions that favor different tridecameric Al polycations: the 'flat' Al_{13} (discussed below) containing only octahedral aluminum forms at pH-2-3, the Keggin Al_{13} forms at pH 4-5. However, deprotonation of a Zn-H_2O complex is considerably less favorable than an Al-H_2O complex, discussed later in relation to pKa's of metal-bound water. On the other hand, structural and related computational studies of Zn in protein complexes, for example, shows a preference for tetrahedral coordination.(Dudev and Lim, 2000)

Table 2. Relative electronic bonding energies between different homonuclear Al Keggin structures, comparing the stabilization effect of ZnO_4 compared to AlO_4 in the tetrahedral center.

	ΔE (kJ.mol⁻¹)	
	M=Al(III)	**M=Zn(II)**
?-$[MO_4@Al_{12}(OH)_{24}(H_2O)_{12}]^{7+/6+}$	**+44.2**	**+85.6**
?-$[MO_4@Al_{12}(OH)_{24}(H_2O)_{12}]^{7+/6+}$	**+19.4**	**+56.5**
?-$[MO_4@Al_{12}(OH)_{24}(H_2O)_{12}]^{7+/6+}$	**0**	**0**

Solution Characterization

Zn dissolution in an acidic metal nitrate solution to drive condensation of monomers to clusters was first demonstrated for synthesis of the "flat" Al_{13} cluster $[Al_{13}(OH)_{24}(H_2O)_{24}]^{15+}$ from $Al(NO_3)_3$.(Wang et al., 2011) The acidity of the reaction solution prior to adding zinc (pH=2.2) results from deprotonation of water molecules bound to the metal cations (M=AlCr):

$$M(H_2O)_6^{3+} \rightarrow yM(H_2O)_{6-x}(OH)_x^{2+} + (y\times x)H^+ \quad (1)$$

where y is some fraction of the total metal cation concentration. In this reaction, Zn metal could reduce either H^+ or NO_3^- with the following potentials:

$$Zn^0 \rightarrow Zn^{2+} + 2e^- \quad (-0.76\ V) \quad (2)$$
$$2H^+ + 2e^- \rightarrow H_2 \quad (0\ V) \quad (3)$$
$$NO_3^- + 3H^+ + 2e^- \rightarrow HNO_2^- + H_2O \quad (0.94) \quad (4)$$

Reaction 3 & 4 both consume protons and increase the pH, and the reduction potential suggests reaction 3 likely dominates over reaction 4. The pH increases in the reaction solution with increased zinc metal addition (**fig. 2a, Table SI-19**). With increased Zn addition that drives equation 1 to the right as protons are consumed, condensation (eq. 5) or bridging (eq. 6) occurs between hydrated and partially deprotonated metal cations, i.e.:

$$2M(H_2O)_5(OH)^{2+} \rightarrow [(H_2O)_5M\text{-}O\text{-}M(H_2O)_5]^{4+} + H_2O \quad (5)$$
$$2M(H_2O)_5(OH)^{2+} + H^+ \rightarrow [(H_2O)_5M\text{-}OH\text{-}M(H_2O)_5]^{3+} + H_2O \quad (6)$$

where M=Al, Cr, Zn. Due to the acidity of the reaction solution and the formula of the isolated cluster containing bridging hydroxyls, reaction (6) is expected to dominate. Using a rounded formula for $Zn(CrAl)_{12}$ we can write a balanced reaction as follows:

$$2[Zn(H_2O)_6]^{2+} + 5[Al(H_2O)_6]^{3+} + 7[Cr(H_2O)_6]^{3+} \rightarrow Zn(H_2O)_3[ZnO_4Al_5Cr_7(OH)_{24}(H_2O)_{12}]^{8+} + 32H^+ + 41H_2O \quad (7)$$

After 2 weeks of allowing the solution to evaporate in open air at room temperature, the pH drops from 3 to 2, and the blue-green crystals of $Zn(CrAl)_{12}$ are observed. The decrease in pH is owed to the release of protons upon cluster assembly (eq. 7) and increase in solution concentration with evaporation. The reaction solutions with variable zinc concentration were characterized by SAXS. With increasing zinc concentration, scattering intensity increases, indicating linking of metal cations to form larger dissolved species; i.e. eq. 5, 6, 7. (**fig. 2a, SI fig. 6**) We prepared a control experiment by dissolving Zn nitrate in the Al/Cr nitrate solution instead of zinc metal (control 5, **Table SI19**). This solution did not exhibit the increase in scattering intensity (**SI, fig. 6**) that is consistent with the hypothesis that oxidative dissolution of Zn^0 drives pH increase, leading to hydrolysis and condensation reactions. On the other hand, X-ray scattering intensity of the reaction solution decreases with aging. (fig. **SI8, fig. 2b**), consistent with loss of the larger scattering species (as crystallization begins).

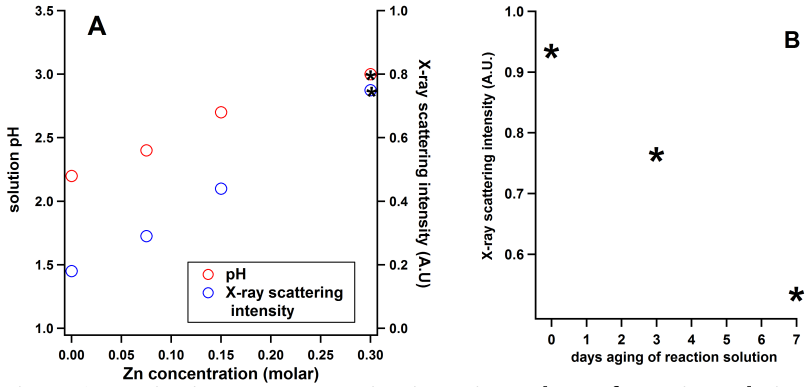

Figure 2. Monitoring X-ray scattering intensity and pH of reaction solutions. A) Reaction solution pH and X-ray scattering intensity (at q=0.1 Å^{-1}, see SI fig. 6) as a function of Zn concentration. The * denotes the optimal Zn concentration from which $Zn(CrAl)_{12}$ were obtained. B) X-ray scattering intensity (at q=0.1 Å^{-1}, see fig. SI8) of the *-solution in fig. 2B with aging.

Despite the qualitative increase in scattering intensity with increased Zn to drive hydrolysis, we were surprised that the SAXS data of the reaction solutions never indicated formation of a fully intact cluster, even at the point where $Zn(CrAl)_{12}$ crystals were abundant. In fact, the scattering is very weak, and this is emphasized in **SI fig. 7** of the data without background subtraction, allowing comparison of the scattering intensity with the solvent (water) peak.

However, isolating the crystals and redissolving them in water (**fig. 3**) led to scattering expected and usually observed in solutions of fully formed clusters. X-ray scattering of dissolved $Zn(CrAl)_{12}$ crystals is more similar to that of simulated $Zn(CrAl)_{12}$, as is the radii of gyration R_g (experiment) = 4.1 Å and R_g (simulated) = 3.9 Å determined by a Guinier analysis (between q=0.25-0.35 Å^{-1}). On the other hand, the Guinier analyses of all reaction solution scattering curves yielded R_g = 2.7 Å (SI fig 8, R_g measured between q=0.3-0.5 Å^{-1}). However, the intensity of the initial scattering decreased with increasing time and decreasing pH (**fig. 2**); meaning the size of the species remained constant while the concentration varied. In summary, while X-ray scattering suggested hydrolysis and condensation reactions occurred in the reaction solutions, full cluster formation was never observed prior to or in

tandem with crystallization, which was unexpected based on our experience with other metal-oxo cluster systems.(Falaise and Nyman, 2016; Goberna‐Ferrón et al., 2016; Sadeghi et al., 2015) For an additional control experiment, we prepared a solution of the Al_{13} Keggin ion, per the well-known synthesis.(Johansson, 1960) In this synthesis, 2.6 equivalents of NaOH are added dropwise to a heated aqueous solution of 0.1 molar aluminum nitrate. This solution indeed yielded X-ray scattering expected from a solution of fully-formed clusters. (**fig. 4**) Note, this reaction solution contains ~1/10th concentration of the cluster-forming metal, compared to the optimal synthesis of $Zn(CrAl)_{12}$. This is an important point that is discussed later.

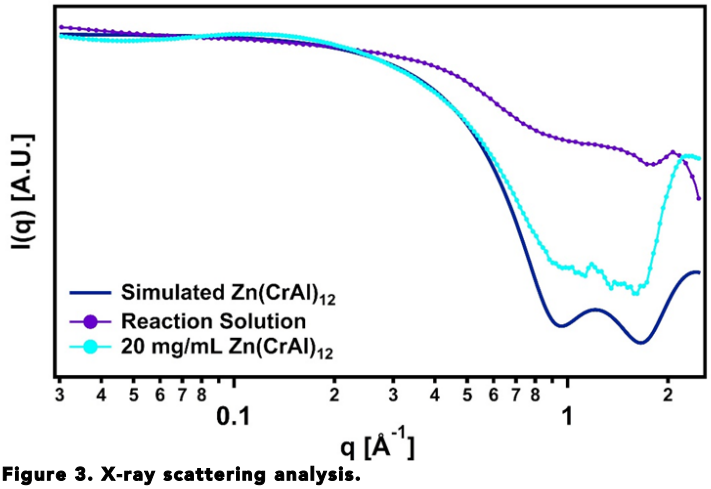

Figure 3. X-ray scattering analysis.
Simulated and experimental scattering curves of $Zn(CrAl)_{12}$ reaction solution 4, pH-3.0, day 1 of aging (Table SI19) and solution of dissolved crystals. Intensity [I(q)] is normalized for ease of comparison. $Zn(CrAl)_{12}$ crystals were actively growing from the reaction solution.

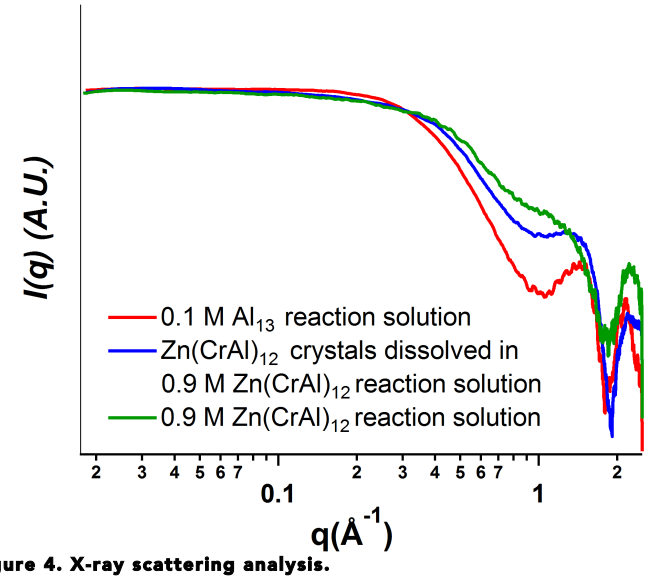

Figure 4. X-ray scattering analysis.
Comparing the scattering curves of the reaction solutions of $Zn(CrAl)_{12}$ to that of Keggin Al_{13}, and crystals of $Zn(CrAl)_{12}$ redissolved in a fresh reaction solution. I_0 intensities are scaled to match for ease of comparison.

Electrospray ionization mass spectrometry (ESI-MS) gave an independent assessment of the reaction solutions. Even at the point of saturation and growth of $Zn(CrAl)_{12}$ crystals, ESI-MS reveals predominantly aqua monomers of Al, Zn, and Cr

(Supplementary **Table 20**) and dimers of Al (**Fig. 5a**, Supplementary Fig. 9), with small error, ± 0.001, between experimental and calculated mass/charge ratios of assigned peaks. The spectrum in figure 5b was collected for reaction solution 4 (Table SI19) at pH-3.0 with one day of aging. Spectra were collected every day until crystallization, and no change was observed in the identified species. ESI-MS (**Fig. 5b**) $Zn(CrAl)_{12}$ crystals dissolved in water shows a complicated mixture of clusters with a range of Cr:Al ratios, representing parent clusters and their daughter ionization fragments. The tridecamer with and without the Zn-cap (**Supplementary Table 21**) is observed. The natural isotopic distribution of both Zn and Cr renders signature peak envelopes that could be simulated, greatly improving confidence in species identification in both the reaction and dissolved-cluster solutions (**Supplementary Figs. 9 & 10**). These data show 1) The Cr:Al ratios of the observed compositions correlate well with the bulk composition determined from structure, electron-microprobe, and theory, and 2) Clusters with higher Cr content are more extensively fragmented by the ionization process, providing evidence for their lower kinetic stability.(Miras et al., 2009; Molina et al., 2015) In contrast to the reaction solutions, clusters are readily detected in solutions prepared by dissolution of $Zn(CrAl)_{12}$ crystals. These data confirmed our SAXS observations: clusters are not present in the reaction solutions at the point of saturation and crystallization of $Zn(CrAl)_{12}$. Together, ESI-MS and SAXS provide a consistent picture of a reaction solution dominated by monomers rather than clusters and a solution of dissolved crystals characterized by largely intact clusters.

However, we cannot ignore that monomers are also observed in solutions of dissolved $Zn(CrAl)_{12}$ crystals. While ESI-MS peak intensities do not reliably quantify species concentrations, the ratio of cluster-peak intensity to monomer-peak intensity is ~1.6. Likewise, we cannot ignore the mismatch between the calculated and experimental scattering data in figure 3, particularly between 0.5-0.8 $Å^{-1}$. The shallower slope of the experimental scattering curve indicates smaller species that scatter at higher q, such as the monomers observed in the mass spectral data. These observations evidence that the clusters are not entirely stable in neat water. However, aging of the solution does not result in any major change.

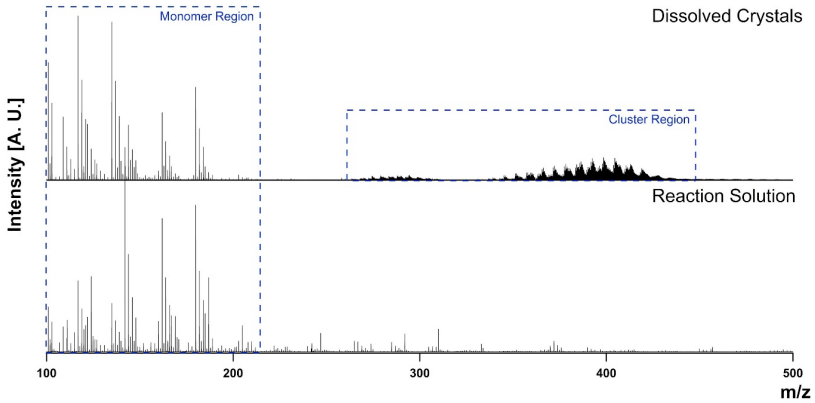

Figure 5. Electrospray ionization mass spectrometry (ESI-MS) analysis.
(A) $Zn(CrAl)_{12}$ crystals. (B) Reaction solution #4, one day of aging, pH-3 (see Table SI19).

DISCUSSION

Proposed pathway $Zn(CrAl)_{12}$ cluster growth

How do $Zn(CrAl)_{12}$ crystals grow from a saturated solution when clusters are not detected in the reaction solution? Perhaps the clusters are highly insoluble in the

reaction solution – as they form, they may be rapidly consumed via crystal growth. To test solubility, we submerged $Zn(CrAl)_{12}$ crystals in a reaction solution. The crystals dissolved quickly, and SAXS measurements revealed that the $Zn(CrAl)_{12}$ clusters revert to small polydisperse species, shown in figure 4. This result is consistent with the acidity constants of the aqua ions:

$$pK_a\ [Zn(H_2O)_6]^{2+} = 9$$
$$pK_a\ [Al(H_2O)_6]^{3+} = 5$$
$$pK_a\ [Cr(H_2O)_6]^{3+} = 4$$

The Zn aqua ion is least acidic, the Cr aqua ion most. Based on the pK_a values of all the metals and the low pH of the reaction solution (2-3), the bridging hydroxyl linkages are expected to hydrolyze, which would then dismantle the clusters. Consequently, the reaction solution does not support fully formed clusters.

Besides pH, we hypothesize NO_3^-(aq) concentration also orchestrates cluster formation. $Zn(CrAl)_{12}$ crystals only grow with evaporation – a capped solution does not produce crystals. Based on electrochemical potentials, Zn metal is expected to primarily reduce H^+(aq). Accordingly, the NO_3^-(aq) concentration remains constant and high throughout the Zn dissolution process. This high concentration further inhibits condensation. To reduce the NO_3^-(aq), we heated the reaction solution in a distillation setup to rapidly evolve nitrate as the H_2O-HNO_3 azeotrope (b.p. = 85 °C at 1 atm). The distillate tests acidic with a pH strip, and its Raman spectrum matches that of 15.7 N HNO_3(aq), see **fig. SI-11**. These results show HNO_3(aq) evolves as expected via azeotropic evaporation. The controlled reduction in NO_3^-(aq) concentration also prompts and expedites crystal growth.

Due to loss of HNO_3(aq) on heating, the reaction solution pH is expected to increase, but it decreases from 3 to 2. Solution hydrolysis, eq. (1), and condensation reactions, eqs. (5), (6), and (7), reduce the pH. ESI-MS data in Figure **SI6** (reaction #4) show condensation produces mixed metal dimers; see also **fig. 6** and **Table SI22**. Similarly, SAXS data in **fig. SI-12** reveal weak scattering and average R_g = 2.7 Å over the q range 0.3-0.5 $Å^{-1}$, results consistent with the ESI-MS study. Heating may be expected to produce some uncontrolled condensation and hydroxide precipitation. However, with heating, we observe only limited solution cloudiness as the characteristic blue crystals of $Zn(CrAl)_{12}$ grow. SAXS data reveal a change in scattering intensity below q = 0.1 $Å^{-1}$, consistent with aggregation and the observed cloudiness of the solution. Also, an increase in the slope of the scattering curves near q = 1 $Å^{-1}$ at elevated temperatures indicates increasing condensation products, consistent with the ESI-MS results. With heat, the crystals grow in one day compared with several weeks for room-temperature evaporation.

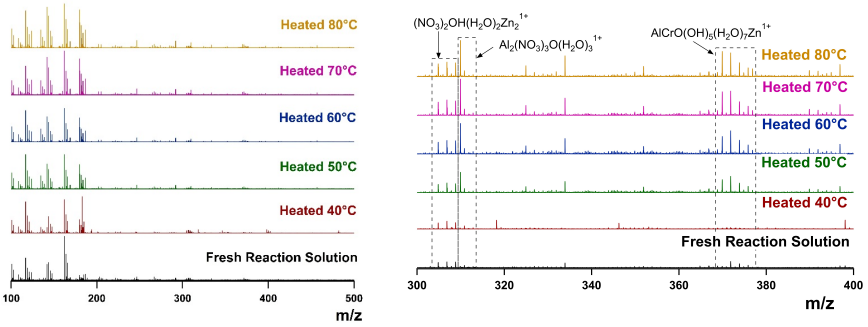

Figure 6. ESI MS of heated reaction solutions.
Left: full spectral range in which peaks are observed, right: zoomed into the region where clusters are

observed in a solution of redissolved crystals.

During the initial stages of $Zn(CrAl)_{12}$ synthesis by Zn metal dissolution, we suggest the combination of low pH (~2) and high nitrate concentration hinders complete cluster assembly. Instead, monomeric aqua ions and small oligomers exist and form in the reaction solution. Persistence of larger clusters in solution commonly produce aggregation and precipitation of metal oxide hydroxides. For example, iron oxide and calcium carbonate readily precipitate from aqueous solutions with very low concentrations of cations and carbonate, following observation of clusters in solution.(Gebauer et al., 2014; Gebauer et al., 2008) These solids precipitate from pre-nucleation clusters at concentrations below 10 mM metal. The conventional Al_{13} Keggin synthesis with NaOH(aq) requires relatively low metal concentrations (0.1 molar), as synthesis with concentrated solutions near 0.9 M Al produces aggregates and precipitates, as does the analogous NaOH(aq) addition to 0.9 M Zn/Cr/Al nitrate solutions. These syntheses highlight the importance of a preparative strategy to prevent aggregation in the bulk solution. We have done so with the $Zn(CrAl)_{12}$ synthesis at 0.9 M metal through 1) pH regulation via Zn dissolution to minimize rapid, uncontrolled hydrolysis and condensation reactions and 2) controlled nitrate evolution via azeotropic evaporation.

Finally, we consider *where* the $Zn(CrAl)_{12}$ clusters assemble and the crystals nucleate, if not in the bulk solution. We suggest two possibilities: 1) The clusters nucleate and grow directly on the surface of the container from monomers and small, oligomeric species in the bulk solution, and 2) Pre-nucleation clusters or complete $Zn(CrAl)_{12}$ clusters form at the water-air interface.

We grew crystals in different types of containers, i.e., glass, Teflon, and plastic. We observed no difference in crystal morphology, growth rate, or composition. Also, we only observe crystals at the bottom of each container and on the surface of the solution, suggesting crystals may not nucleate on the container surfaces. Consequently, proposal 1) is not supported by observations.

As for proposal 2), Antonio and co-workers (Bera et al., 2015) recently characterized both the surface and the bulk of a drop of an aqueous $Er(NO_3)_3$ solution by X-ray absorption spectroscopy. The spectra show clusters exist near the surface, while only monomers exist in the bulk. Ions, including hydrolyzed metal aqua ions tend to concentrate near the aqueous-air interface (Ghosal et al., 2005), which then favors condensation and cluster formation. In the $Zn(CrAl)_{12}$ system, we propose similar effects produce high concentrations of hydrolyzed aqua ions near the solution surface. Their condensation is enhanced by reduction of the nitrate concentration via evaporation of the nitric-acid-water azeotrope. Collectively, these processes likely produce low concentrations of high nuclearity clusters that then can contribute to crystal growth. We propose X-ray absorption measurements may reveal the presence of clusters near the water-air interface in the $Zn(CrAl)_{12}$ system. These measurements and others will help inform our understanding of the pathways by which such clusters form and crystallize.

SUPPLEMENTAL INFORMATION

Supplementary information includes Tables 1-22, Figures 1-11, and Crystallographic information file (CSD-428054, ZnCrAl12.cif)

AUTHOR CONTRIBUTIONS

W.W. performed and optimized the initial synthesis and crystal growth; L.B.F. and S.G.F carried out the SAXS and ESI MS characterizations and heated reaction studies; N.A.G.B performed computational studies; L.N.Z. carried out single crystal X-ray diffraction; C.B., M.N. and D.A.K. designed the experiments, supervised the work, discussed the data and co-wrote the manuscript.

ACKNOWLEDGMENTS

The experimental work at OSU was supported by the National Science Foundation under Grant No. CHE-1102637 in support of the Center for Sustainable Materials Chemistry, a Phase-II Center for Chemical Innovation. The computational work performed at ICIQ was supported by the Spanish Ministerio de Economia y Competitividad (MINECO) through project CTQ2011-29054-C02-02 and CTQ2014-52824-R, by the Generalitat de Catalunya project 2014SGR409, and by the ICIQ Foundation. N.A.G.B thanks the Marie Curie/COFUND scheme ref. 291787-ICIQ-IPMP for funding. The Severo Ochoa Excellence Accreditation (SEV-2013-0319) and the COST Action CM1203 "Polyoxometalate Chemistry for Molecular Nanoscience (PoCheMoN)" are gratefully acknowledged.

REFERENCES

1. Ako, A.M., Hewitt, I.J., Mereacre, V., Clerac, R., Wernsdorfer, W., Anson, C.E., and Powell, A.K. (2006). A ferromagnetically coupled Mn-19 aggregate with a record S=83/2 ground spin state. Angew Chem Int Edit *45*, 4926-4929.
2. Allouche, L., Huguenard, C., and Taulelle, F. (2001). 3QMAS of three aluminum polycations: Space group consistency between NMR and XRD
3. J Phys Chem Sol *62*, 1525-1531.
4. Anderson, J.T., Munsee, C.L., Hung, C.M., Phung, T.M., Herman, G.S., Johnson, D.C., Wager, J.F., and Keszler, D.A. (2007). Solution-processed HafSOx and ZircSOx inorganic thin-film dielectrics and nanolaminates. Adv Funct Mater *17*, 2117-2124.
5. Baes, C.F., and Mesmer, R.E. (1976). The Hydrolysis of Cations (New York: John Wiley and Sons Inc.).
6. Barats, D., Leitus, G., Popovitz-Biro, R., Shimon, L.J.W., and Neumann, R. (2008). A Stable "End-On" Iron(III)-Hydroperoxo Complex in Water Derived from a Multi-Iron(II)-Substituted Polyoxometalate and Molecular Oxygen. Angew Chem Int Edit *47*, 9908-9912.
7. Bashan, A., and Yonath, A. (2008). The linkage between ribosomal crystallography, metal ions, heteropolytungstates and functional flexibility. J Mol Struct *890*, 289-294.
8. Baskar, V., Shanmugam, M., Helliwell, M., Teat, S.J., and Winpenny, R.E.P. (2007). Reverse-keggin ions: Polycondensation of antimonate ligands give inorganic cryptand. J Am Chem Soc *129*, 3042-+.
9. Baumgartner, J., Dey, A., Bomans, P.H.H., Le Coadou, C., Fratzl, P., Sommerdijk, N.A.J.M., and Faivre, D. (2013). Nucleation and growth of magnetite from solution. Nat Mater *12*, 310-314.
10. Becke, A.D. (1988a). Density-functional exchange-energy approximation with correct asymptotic behaviour. Phys Rev A *38*, 3098-3100.
11. Becke, A.D. (1988b). A multicenter numerical integration scheme for polyatomic molecules. J Chem Phys *88*, 2547-2553.

12. Bera, M.K., Luo, G., Schlossman, M.L., Soderholm, L., Lee, S., and Antonio, M.R. (2015). Erbium (III) Coordination at the Surface of an Aqueous Electrolyte. The Journal of Physical Chemistry B *119*, 8734-8745.
13. Bradley, S.M., Lehr, C.R., and Kydd, R.A. (1993). Base Hydrolysis of aqueous chromium (III) solutions-on the existence of $Cr(OH)_4^-$ and speculation regarding the new chromium polyoxocation. J Chem Soc-Dalton Trans, 2415-2420.
14. Busche, C., Vila-Nadal, L., Yan, J., Miras, H.N., Long, D.L., Georgiev, V.P., Asenov, A., Pedersen, R.H., Gadegaard, N., Mirza, M.M., *et al.* (2014). Design and fabrication of memory devices based on nanoscale polyoxometalate clusters. Nature *515*, 545-549.
15. Casey, W.H. (2006). Large Aqueous Aluminum Hydroxide Molecules. Chem Rev *106*, 1-16.
16. Donovan, J.J., and Tingle, T.N. (1996). An improved mean atomic number background correction for quantitative microanalysis. Microscopy and Microanalysis *2*, 1-7.
17. Dudev, T., and Lim, C. (2000). Tetrahedral vs octahedral zinc complexes with ligands of biological interest: A DFT/CDM study. J Am Chem Soc *122*, 11146-11153.
18. Falaise, C., and Nyman, M. (2016). The key role of U28 in aqueous self-assembly of uranyl peroxide nanocages Chemistry A European Journal.
19. Gebauer, D., Kellermeier, M., Gale, J.D., Bergstrom, L., and Colfen, H. (2014). Pre-nucleation clusters as solute precursors in crystallisation. Chem Soc Rev *43*, 2348-2371.
20. Gebauer, D., Volkel, A., and Colfen, H. (2008). Stable Prenucleation Calcium Carbonate Clusters. Science *322*, 1819-1822.
21. Ghosal, S., Hemminger, J.C., Bluhm, H., Mun, B.S., Hebenstreit, E.L., Ketteler, G., Ogletree, D.F., Requejo, F.G. and Salmeron, M., (2005). Electron spectroscopy of aqueous solution interfaces reveals surface enhancement of halides. Science, *307*(5709), 563-566.
22. Goberna‐Ferrón, S., Park, D.H., Amador, J.M., Keszler, D.A., and Nyman, M. (2016). Amphoteric Aqueous Hafnium Cluster Chemistry. Angewandte Chemie *128*, 6329-6332.
23. Habraken, W.J.E.M., Tao, J.H., Brylka, L.J., Friedrich, H., Bertinetti, L., Schenk, A.S., Verch, A., Dmitrovic, V., Bomans, P.H.H., Frederik, P.M., *et al.* (2013). Ion-association complexes unite classical and non-classical theories for the biomimetic nucleation of calcium phosphate. Nat Commun *4*.
24. Hirshfeld, F.L. (1977). Bonded-atom fragments for describing molecular charge densities. Theor Chim Acta *44*, 129-138.
25. Ilavsky, J., and Jemian, P.R. (2009). Irena: tool suite for modeling and analysis of small-angle scattering. J Appl Crystallogr *42*, 347-353.
26. Izarova, N.V., Kondinski, A., Vankova, N., Heine, T., Jäger, P., Schinle, F., Hampe, O., and Kortz, U. (2014). The Mixed Gold–Palladium Polyoxo‐Noble‐Metalate $[NaAu^{III}_4Pd^{II}_8O_8(AsO_4)8]^{11-}$. Chemistry–A European Journal *20*, 8556-8560.
27. Izarova, N.V., Vankova, N., Heine, T., Biboum, R.N., Keita, B., Nadjo, L., and Kortz, U. (2010). Polyoxometalates made of gold: the polyoxoaurate $[Au^{III}_4As^{V}_4O20]^{8-}$. Angewandte Chemie International Edition *49*, 1886-1889.
28. Johansson, G. (1960). The crystal structure of a basic aluminum selenate. Acta Chemica Scandinavica *14*, 771-773.

29. Kamata, K., Yonehara, K., Sumida, Y., Yamaguchi, K., Hikichi, S., and Mizuno, N. (2003). Efficient epoxidation of olefins with >= 99% selectivity and use of hydrogen peroxide. Science *300*, 964-966.
30. Lee, I.S., Long, J.R., Prusiner, S.B., and Safar, J.G. (2005). Selective precipitation of prions by polyoxometalate complexes J Am Chem Soc *127*, 13802-13803.
31. Llordes, A., Garcia, G., Gazquez, J., and Milliron, D.J. (2013). Tunable near-infrared and visible-light transmittance in nanocrystal-in-glass composites. Nature *500*, 323-+.
32. Lokare, K.S., Frank, N., Braun ‐ Cula, B., Goikoetxea, I., Sauer, J., and Limberg, C. (2016). Trapping Aluminum Hydroxide Clusters with Trisilanols during Speciation in Aluminum (III)–Water Systems: Reproducible, Large Scale Access to Molecular Aluminate Models. Angewandte Chemie.
33. Miras, H.N., Wilson, E.F., and Cronin, L. (2009). Unravelling the complexities of inorganic and supramolecular self-assembly in solution with electrospray and cryospray mass spectrometry. Chem Commun, 1297-1311.
34. Molina, P., Sures, D., Miró, P., Zakharov, L., and Nyman, M. (2015). Bridging the opposite chemistries of tantalum and tungsten polyoxometalates. Dalton T *44*, 15813-15822.
35. Newton, G.N., Yamashita, S., Hasumi, K., Matsuno, J., Yoshida, N., Nihei, M., Shiga, T., Nakano, M., Nojiri, H., Wernsdorfer, W.*, et al.* (2011). Redox-Controlled Magnetic {Mn-13} Keggin Systems. Angew Chem Int Edit *50*, 5715-5719.
36. Nyman, M., and Burns, P.C. (2012). A comprehensive comparison of transition-metal and actinyl polyoxometalates. Chem Soc Rev *41*, 7354-7367.
37. Oleksak, R.P., Ruther, R.E., Luo, F.X., Fairley, K.C., Decker, S.R., Stickle, W.F., Johnson, D.W., Garfunkel, E.L., Herman, G.S., and Keszler, D.A. (2014). Chemical and Structural Investigation of High-Resolution Patterning with HafSOx. Acs Appl Mater Inter *6*, 2917-2921.
38. Parker, W.O., Millini, R., and Kiricsi, I. (1997). Metal substitution in Keggin-type tridecameric aluminum-oxo-hydroxy clusters. Inorg Chem *36*, 571-575.
39. Perdew, J.P. (1986a). Density-functional approximation for the correlation energy of the inhomogeneous electron gas. Phys Rev B *33*, 8822-8824.
40. Perdew, J.P. (1986b). Erratum: Density-functional approximation for the correlation energy of the inhomogeneous electron gas. Phys Rev B *34*, 7406.
41. Pope, M.T. (1983). Heteropoly and Isopoly Oxometalates (New York: Springer-Verlag).
42. Rhule, J.T., Hill, C.L., and Judd, D.A. (1998). Polyoxometalates in medicine. Chemical Reviews *98*, 327-357.
43. Rowsell, J., and Nazar, L.F. (2000). Speciation and thermal transformation in alumina sols: Structures of the polyhydroxyoxoaluminum cluster $[Al_{30}O_8(OH)_{56}(H_2O)_{26}]^{(18+)}$ and its delta-Keggin moiete. J Am Chem Soc *122*, 3777-3778.
44. Sadeghi, O., Zakharov, L.N., and Nyman, M. (2015). Aqueous formation and manipulation of the iron-oxo Keggin ion. Science *347*, 1359-1362.

45. Son, J.H., Park, D.H., Keszler, D.A., and Casey, W.H. (2015). Acid-Stable Peroxoniobophosphate Clusters To Make Patterned Films. Chem-Eur J *21*, 6727-6731.
46. Stewart, T.A., Trudell, D.E., Alam, T.M., Ohlin, C.A., Lawler, C., Casey, W.H., Jett, S., and Nyman, M. (2009). Enhanced Water Purification: A Single Atom Makes a Difference. Environ Sci Technol *43*, 5416-5422.
47. Stracke, J.J., and Finke, R.G. (2011). Electrocatalytic Water Oxidation Beginning with the Cobalt Polyoxometalate $[Co_4(H_2O)_2(PW_9O_{34})_2]^{10-}$: Identification of Heterogeneous CoO_x as the Dominant Catalyst. J Am Chem Soc *133*, 14872-14875.
48. Sun, Y.-Q., Mei, H.-X., Zhang, H.-H., Chen, Y.-P., and Sun, R.-Q. (2011). Unique (3, 12)-Connected Inorganic Lanthanide Cluster Polymer Based on Octahedral Hexanuclear Europium Hydroxide Clusters and Sulfate Anions: Synthesis, Structure, and Luminescence. Journal of Cluster Science *22*, 279-288.
49. Tiede, D.M., Zhang, R.T., Chen, L.X., Yu, L.H., and Lindsey, J.S. (2004). Structural characterization of modular supramolecular architectures in solution. J Am Chem Soc *126*, 14054-14062.
50. Van der Sluis, P., and Spek, A. (1990). BYPASS: an effective method for the refinement of crystal structures containing disordered solvent regions. Acta Crystallographica Section A: Foundations of Crystallography *46*, 194-201.
51. Van Lenthe, E., and Baerends, E.J. (2003). Optimized Slater-type basis sets for the elements 1–118. J Comput Chem *24*, 1142-1156.
52. van Lenthe, E., Baerends, E.J., and Snijders, J.G. (1993). Relativistic regular two-component Hamiltonians. J Chem Phys *99*, 4597-4610.
53. van Lenthe, E., Ehlers, A.E., and Baerends, E.J. (1999). Geometry optimizations in the zero order regular approximation for relativistic effects J Chem Phys *110*, 8943-8953.
54. Wang, W., Wentz, K.M., Hayes, S.E., Johnson, D.W., and Keszler, D.A. (2011). Synthesis of the Hydroxide Cluster $[Al\text{-}_3(\mu_3\text{-}OH)_6(\mu_3\text{-}OH)_{18}(H_2O)_{24}]^{(15+)}$ from an Aqueous Solution. Inorg Chem *50*, 4683-4685.
55. Winkler, J.R., and Gray, H.B. (2012). Electronic Structures of Oxo-Metal Ions. Struct Bond *142*, 17-28.
56. Wylie, E.M., Peruski, K.M., Weidman, J.L., Phillip, W.A., and Burns, P.C. (2014). Ultrafiltration of Uranyl Peroxide Nanoclusters for the Separation of Uranium from Aqueous Solution. Acs Appl Mater Inter *6*, 473-479.
57. Yin, Q.S., Tan, J.M., Besson, C., Geletii, Y.V., Musaev, D.G., Kuznetsov, A.E., Luo, Z., Hardcastle, K.I., and Hill, C.L. (2010). A Fast Soluble Carbon-Free Molecular Water Oxidation Catalyst Based on Abundant Metals. Science *328*, 342-345.
58. Zhang, R.T., Thiyagarajan, P., and Tiede, D.M. (2000). Probing protein fine structures by wide angle solution X-ray scattering. J Appl Crystallogr *33*, 565-568.